RSC Advances

ROYAL SOCIETY OF CHEMISTRY

www.rsc.org/advances

Vibrational analysis and chemical activity of paracetamol-oxalic acid cocrystal based on monomer and dimer calculations:DFT and AIM approach

Karnica Srivastava[1], Manishkumar R. Shimpi[2], Anubha Srivastava[1], Poonam Tandon[*1],Kirti Sinha[1] and Sitaram P. Velaga[2]

[1]*Physics Department, University of Lucknow, Lucknow 226 007, India*
[2]*Department of Health Sciences Luleå University of Technology, S-971 87, Luleå, Sweden*

This submission was created using the RSC Article Template (DO NOT DELETE THIS TEXT)
(LINE INCLUDED FOR SPACING ONLY - DO NOT DELETE THIS TEXT)

The study of structural and spectral characteristics of paracetamol-oxalic acid (PRA-OXA) cocrystal has been carried out using two models (monomer and dimer), with the aim to understand the supramolecular structure and intramolecular interactions within cocrystal. The cocrystal has been characterized by infrared and Raman spectroscopy combined with quantum chemical calculations. Molecular electrostatic potential surface (MEPS), frontier orbital analysis and electronic reactivity descriptors were used to understand the role of interactions involved in affecting the chemical reactivity of individual molecule in cocrystal. It is observed that C=O, N-H and O-H groups of paracetamol are involved in hydrogen bonds to form cocrystals. NBO analysis suggests that the two type of interactions LP(1)(N8)→π*(C9-O10) and LP (2)(O10)→σ*(O25-H28) are responsible for stability of the molecule. AIM analysis suggested that the non-covalent interactions are moderate in nature. The calculated HOMO-LUMO energies reveal that the charge transfer occurs within the cocrystal. Chemical reactivity parameters show that cocrystal is more active than paracetamol.

1. Introduction

Pharmaceutical cocrystals can be defined as crystalline materials comprised of an active pharmaceutical ingredient (API) and one or more unique co-crystal formers, which are solids at room temperature. Pharmaceutical cocrystals have attracted phenomenal interest in recent years due to their potential to improve the physicochemical properties of drug substances such as solubility, dissolution rate, stability hygroscopisity, and compressibility without alternating their pharmacological behavior[1,2]. Cocrystal are formed through different types of interactions, including hydrogen bonding, pi-stacking, and van der Waals forces. Crystal engineering principles based on supramolecular synthon approach has been a powerful tool in the design of cocrystal[3-5]. Supramolecular synthons can be formed between similar (homo) or different (hetero) functional groups such as carboxylic acids, amides and alcohols[6]. The strong hydrogen bonds include (N-H····O), (O-H····O), (N-H····N) and (O-H····N) whilst weak hydrogen bonds involves–C-H····O and C-H····N[7].

Paracetamol known as acetaminophen or PRA, chemically named N-acetyl-p-aminophenol, is widely used over-the counter analgesic (pain reliever) and antipyretic (fever reducer)[8,9]. It is used to treat many conditions such as headache, muscle aches, arthritis, backache, cold and fevers. Paracetamol has two well known polymorphic forms, monoclinic (form I)and orthorhombic (form II). The parallel packing of flat hydrogen bonded layers in the metastable form[10] II results in compaction properties superior to the thermodynamic stable form I which contains corrugated hydrogen bonded layers of molecules. Marketed paracetamol tablet consists of thermodynamic stable monoclinic (form I) accompanied by a large loading of binder that prevents chipping and disintegration[11].

Hence cocrystallization with oxalic acid (alpha) is used as a strategy to generate layered solid form of paracetamol that would be thermodynamically stable and exhibit optimal mechanical properties.Structural analysis revealed that paracetamol (API) molecule is hydrogen bonded to four neighboring oxalic acid (co-former) molecule through heteromeric interaction forming paracetamol-oxalic acid (PRA-OXA) cocrystal. Paracetamol acts as a two-fold hydrogen bond donor through amide NH and phenol OH group and two-fold acceptor via the amide C=O and OH group[12].

Recently combined spectroscopic (infrared, Raman or terahertz spectroscopy) and quantum chemical approach has been used to study the structure and hydrogen bonding in pharmaceutical cocrystals[13-15]. Previously in PiMM approach[16-18] the effect of intermolecular interactions on vibrational spectra was evaluated from *ab initio* calculation for several sets of molecular pairs. Approach used in the present work is different from PiMM as here all the nearby interactions are considered in a single model making the calculation much simpler. The FT-IR and Raman spectra of PRA-OXA cocrystal was recorded in solid state and compared with calculated wavenumber of monomer and dimer forms. To improve the vibrational assignments in solid phase, simulations were carried out for dimer form with two additional oxalic acid (alpha) molecules attached to it (dimer+2OXA) so that all the possible nearest neighbor hydrogen bonding interactions can be incorporated. The quantum theory of atoms in molecules (QTAIM) and natural bond (NBO) analysis are used to evaluate the strength and nature of hydrogen bonds in detail. The molecular electrostatic potential surface (MEPS), global and local reactivity descriptors are used to predict the chemical reactivity of PRA-OXA cocrystal in comparison to paracetamol.

2.Experimental

Paracetamol (4-acetaminophenol, monoclinic form) and oxalic acid used was purchased from Sigma-Aldrich (SIGMA-ALDRICH CHEMIE GmbH.). A 10 mL glass vial was charged with 1.5g of paracetamol, 0.9 g of oxalic acid. 2mL of ethyl acetate was added to form slurry. The reaction was allowed to stir for a total of 48 hours, at which time the solids present were isolated by vacuum filtration and air dried at room temperature.

Corresponding author:Tel.+915222782653; Fax: +915222740840, Email: poonam_tandon@yahoo.co.uk, poonam_tandon@hotmail.com. (P. Tandon).

Prepared cocrystal were analysed using DSC and XRPD to validate the product material(As shown in ESI† Fig .S1 and Fig.S2).

Infrared spectra were recorded on a Bruker Vertex 80v FTIR spectrometer equipped with a DLaTGS detector and a Platinum-ATR accessory with a diamond crystal as ATR element. Both a single beam background without sample and single beam spectra of the powered samples were obtained by averaging 128 scans with an optical resolution of 4 cm^{-1}.The resulting interferograms were Fourier transformed using the Mertz phase correction mode, a Blackman-Harris 3-term apodization function, and a zero filling factor of 2.All spectra were recorded under vacuum using the double-side forward-backward acquisition mode.

Raman spectra were recorded using a Raman microscope (Kaiser Optical Systems, Inc., Ann Arbor, MI, USA) with 785 nm laser excitation. The laser power at the solid samples was approximately 100 mW. Spectra were obtained for one 10 s exposure of the charge coupled device (CCD) detector in the wave number range 100–4000 cm^{-1}. The spectrometer was controlled by commercial instrument software (HoloGRAMS, version 4.0, Kaiser Optical Systems, Inc., Ann Arbor, MI, USA).

3. Computational and theoretical details

The electronic structure and optimized geometry of the PRA-OXA (monomer and dimer+2OXA) were computed by the density functional theory (DFT) methods using the Gaussian 09 program[19] package employing 6-311++G(d, p) basis set[20,21] and Becke's three parameter (local, non local, Hartree–Fock) hybrid exchange functional with Lee–Yang–Parr correlation functional (B3LYP)[22-24]. The absolute Raman intensities and infrared absorption intensities were calculated in the harmonic approximation at the same level of theory, as used for the geometry optimization, from the derivatives of the polarizability and dipole moment associated with each normal mode, respectively.

DFT calculations yield Raman scattering amplitudes, which cannot be taken directly to be the Raman intensities. The Raman scattering cross section, $\partial\sigma_j/\partial\Omega$, which are proportional to Raman intensity may be calculated from the Raman scattering amplitude and predicted wave numbers for each normal mode using the relationship[25,26].

$$\frac{\partial\sigma_j}{\partial\Omega} = \left(\frac{2^4\pi^4}{45}\right)\left(\frac{(\nu_o - \nu_j)^4}{1 - \exp\left[\frac{-hc\nu_j}{KT}\right]}\right)\left(\frac{h}{8\pi^2 c\nu_j}\right)S_j \qquad (1)$$

where S_j and ν_j are the scattering activities and the predicted wave numbers, respectively of the jth normal mode, ν_0 is the wave number of the Raman excitation line and h, c and k are universal constants. The calculated Raman and IR intensities were used to convolute each predicted vibrational mode with a Lorentzian line shape (FWHM = 8 cm^{-1}) to produce simulated spectra.

The normal mode analysis was performed and the potential energy distribution (PED) of monomer was calculated along the internal coordinates using localized symmetry using Gar2Ped programme[27,28,29]. For this purpose a complete set of 78 internal coordinates of monomer were defined using Pulay's recommendations[27]. Visualization, graphical presentation and confirmation of calculated data were done by using the ChemCraft and GaussView software[30,31]. An AIM calculation was performed by AIM 2000 program[32].

Natural bond orbital (NBO) analysis has been performed on the molecule at the B3LYP/6-311++G(d,p) level in order to elucidate the intramolecular charge transfer interaction, rehybridization and delocalization of electron density within the molecule. The electron donor orbital, acceptor orbital and the interacting stabilization energy was analyzed using the second-order micro-disturbance theory. The higher value of hyperconjugative interaction energy $E^{(2)}$ results the more

intensive interaction between the electron donor to electron acceptor[33-35].

The hyperconjugative interaction energy was deduced from the second order perturbation approach.

$$E^{(2)} = -q_i\left[\frac{(F_{ij})^2}{\epsilon_j - \epsilon_i}\right] \qquad (2)$$

where, q_i is the donor orbital occupancy, ϵ_i and ϵ_j diagonal elements (orbital energies) and F_{ij} is the off- diagonal NBO Fock- matrix element.

Molecular electrostatic potential surface (MEPS) is also calculated at the same level of theory. Molecular electrostatic potential V(r) generated through the molecules, electrons and nuclei are given by the expression:

$$V(r) = \sum_A \frac{Z_A}{|\vec{R_A} - \vec{r}|} - \int \frac{\rho(\vec{r'})dr'}{|\vec{r'} - \vec{r}|} \qquad (3)$$

where Z_A is the charge on nucleus A, located at R_A and $\rho(r')$ is the electronic density function for the molecule.

The electronic parameters, such as highest occupied molecular orbital (HOMO) energy (E_{HOMO}), lowest unoccupied molecular orbital (LUMO) energy (E_{LUMO}) and band gap energy ($\Delta E=E_{LUMO}-E_{HOMO}$) were described through theoretical calculations. The atomic orbital compositions of the molecular orbitals were obtained by GaussView software[31]. On the basis of energy of frontier orbitals, the different global reactivity descriptors such as electronegativity (χ), chemical potential (μ), global hardness (η), global electrophilicity index (ω) and global softness (S) are computed using equations given below:

$$\chi = -\frac{1}{2}(E_{HOMO} + E_{LUMO}) \qquad (4)$$

$$\mu = -\chi = \frac{1}{2}(E_{HOMO} + E_{LUMO}) \qquad (5)$$

$$\eta = \frac{1}{2}(E_{LUMO} - E_{HOMO}) \qquad (6)$$

$$S = \frac{1}{2\eta} \qquad (7)$$

$$\omega = \frac{\mu^2}{2\eta} \qquad (8)$$

According to Parr et al.[36], electrophilicity index (ω) is a global reactivity index similar to chemical hardness (η) and chemical potential (μ), which is a positive and definite quantity.

For an atom k in a molecule, three kinds of condensed Fukui function for neuclophilic, electrophilic and radical attacks can be obtained using Eq.(9-11) depending upon the type of electron transfer. According to Parr and Yang[37], the sites, which have highest values of Fukui function f(r) are more reactive centers in chemical species.

For nucleophilic attack

$$f_k^+(r) = [q_k(N + 1) - q_k(N)] \qquad (9)$$

For electrophilic attack

$$f_k^-(r) = [q_k(N) - q_k(N - 1)] \qquad (10)$$

For radical attack

$$f_k^0(r) = \frac{1}{2}[q_k(N + 1) - q_k(N - 1)] \qquad (11)$$

where q_k is the gross electronic population of atom k in the molecule.

Local softnesses and electrophilicity indices are calculated using Eq. (12) and (13).

$$s_k^+ = Sf_k^+, s_k^- = Sf_k^-, s_k^0 = Sf_k^0 \qquad (12)$$

$$\omega_k^+ = \omega f_k^+, \quad \omega_k^- = \omega f_k^-, \quad \omega_k^0 = \omega f_k^0 \qquad (13)$$

Associated with the definition of global electrophilicity (ω), an additional and useful relationship accounts for maximum electronic charge ($\triangle N_{max}$) that the electrophile may accept from the surroundings. Here the surroundings may be expressed by either external effects approaching, for instance, as from the interaction with the solvent or simply as field effects coming from the presence of substituent groups present in the molecule.

The maximum electronic charge that the electrophile may accept from the surroundings ($\triangle N_{max}$) may be defined as

$$\Delta N_{max} = -\frac{\mu}{\eta} \qquad (14)$$

If we consider the two molecules A and B approaching each other, the amount of charge transfer between them may be expressed in terms of electrophilicity i.e. electrophilicity charge transfer (ECT)[38] is defined as the difference between the $\triangle N_{max}$ values of interacting molecules (i) if ECT>0, charge flows from B to A (ii) if ECT < 0, charge flows from A to B. ECT is calculated using Eq.(15)

$$ECT = (\Delta N_{max})_A - (\Delta N_{max})_B \qquad (15)$$

where $(\Delta N_{max})_A = -\frac{\mu_A}{\eta_A}$ and $(\Delta N_{max})_B = -\frac{\mu_B}{\eta_B}$

4.Results and discussion:

4.1 Geometry optimization

The initial structure of PRA-OXA (monomer) and PRA-OXA (dimer+2OXA) was taken from the available crystallographic data of PRA-OXA cocrystal, and that for paracetamol (monomer) and oxalic acid monomer from their crystal structures[12,39,40] and further optimized at the level of theory mentioned earlier. The ground state optimized structure of PRA-OXA (monomer), PRA-OXA (dimer+2OXA), paracetamol (monomer) and oxalic acid (monomer) are shown in Fig. 1, Fig. 2, Fig.S3 and Fig. S4, ESI† respectively and the optimized structural parameters of PRA-OXA (monomer and dimer+2OXA) are listed in Table S1, ESI† along with the experimental values obtained from the available crystallographic data[12].

Small deviation in the computed geometrical parameters from those reported in crystallographic data[12] may be due to intermolecular interactions in the crystalline state. The hydroxyl group of oxalic acid forms a hydrogen bond O-H···O=C with the oxygen atom of amide group attached to paracetamol and hydroxyl group of paracetamol forms strong intermolecular hydrogen bond with the oxygen atom of carboxyl group of oxalic acid O-H···O=C resulting in the formation of PRA-OXA cocrystal.
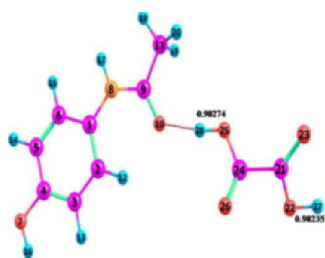
Fig. 1 Optimized structure for monomer of PRA-OXA cocrystal and the atom numbering scheme adopted in this study

As shown in Table S1, ESI† the calculated values of the bond lengths of monomer do not differ more than 0.02Å from the experimental values, except for the bond length, C21-O22,

C21=O23 and C24=O26, which differ from 1.28/1.34, 1.23/1.20, and 1.23/1.20 Å, respectively. Because these bonds are involved in intermolecular hydrogen bonding, which is not taken into account in monomer. The maximum deviation in bond angles is 9° except for the angle C9O10H28, which changes from 117^0 to 129° and O10H28O25, which changes from 157° to 172°. The dihedral angles also do not differ by more than 9° except for the dihedral angle, O10C9C11H19, which changes from -163° to -179°, dihedral angle C9O10H28O25 changes from 70° to -13°, dihedral angle C24O25H28O10 changes from 110° to 170° and the rotation about the bond C21-C24 corresponds to the change in dihedral angle from 178° to -135°. The difference in dihedral angle in monomer is around the bonds involved in hydrogen bonding in cocrystal. In case of dimer+2OXA, as shown in Fig. 2 the geometric parameters of the groups involved in the intermolecular hydrogen bonding, show much smaller deviation from experimental values in comparison to monomer, such as the O7-H16, C24=O26, C4-O7, and O25-H28, which differ from 0.96/0.98, 1.20/1.21,1.36/1.37 and 0.99/1.02. The binding energy of cocrystal formation is computed as the difference between the calculated total energy of the cocrystal and the energies of the API and co-former and found to be 19.51 kcal/mol. The calculated binding energy of cocrystal formation has been corrected for the basis set superposition error (BSSE) via the standard counterpoise method[41] and found to be 18.91 kcal/mol.
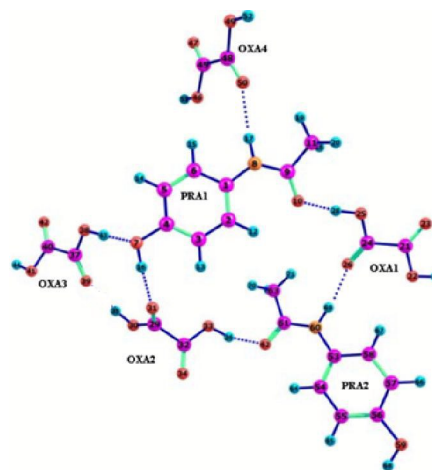
Fig. 2 Optimized structure for dimer+2OXA of cocrystal and the atom numbering scheme adopted in this study.

4.2 Vibrational Assignments

One molecule of PRA-OXA cocrystal has 28 atoms; hence, it gives 78 (3N−6) normal modes of vibrations. All the 78 fundamental vibrations of the cocrystal belongs to the A irreducible representation, are both Raman and IR active. However, the vibrational analysis of paracetamol has already been reported[42] using DFT-B3PW91/6-311++G(d,p) basis set. The present calculation of vibrational wavenumbers and assignments have been done on paracetamol (monomer) and oxalic acid (monomer) individually at B3LYP/6-311++G(d,p), for better understanding of changes in the vibrational spectra resulted due to cocrystal formation. One molecule of paracetamol and oxalic acid has 20 and 8 atoms giving 54 and 18 normal modes of vibrations respectively. Their optimized structures are shown in Fig.S3 and S4, ESI† respectively. The theoretical and observed vibrational wave numbers of paracetamol and oxalic acid along with their PED assignment are shown in Table S2 and S3, ESI†.

Comparison of calculated wavenumbers with experimental values reveals an overestimation due to neglect of anharmonicity present in real system. Since the vibrational wavenumbers obtained from the DFT calculations are higher

than the experimental wave numbers, they were scaled down by 0.9679[43] and a comparison was made with the experimental values. All the calculated wave numbers reported in this study are the scaled values.

Table 1 The Experimental and Theoretical bond length (in Å) and stretching frequency (in cm^{-1}) of the bonds involved in hydrogen bonding

Experimental	O-H (paracetamol)		O-H (oxalic acid)		C=O (oxalic acid)		C=O (paracetamol)		N-H (paracetamol)	
	Bond Length	Stretching frequency	Bond Length	Stretching frequency	Bond Length	Stretching frequency	Bond length	Stretching frequency	Bond length	Stretching frequency
Paracetamol	0.9900	3321 (IR)					1.2397	1651, 1649(IR, Raman)	1.0150	3256 (IR)
Oxalic acid			0.9257, 0.9257	3099 (IR)	1.2071, 1.2071	1749,1739 (IR, Raman)				
Cocrystal	0.9849	3383,3380 (IR , Raman)	0.9827, 0.9823	2999 (IR)	1.2321, 1.2393	1724,1749 (IR,Raman)	1.2426	1655(IR)	1.0094	3344,3346 (IR, Raman)
Calculated										
monomer	0.9629	3712	0.9988, 0.9698	3086,3631	1.2041,1.2015	1764, 1746	1.2329	1643	1.0086	3509
dimer+ 2OXA	0.9841 (PRA1)	3320	1.0163, 0.9696 (OXA1) 1.0127, 0.9850 (OXA4)	2777,3636 (OXA1) 2849,3369 (OXA4)	1.2119,1.1987 (OXA1) 1.2031,1.2187, (OXA4)	1721, 1773 (OXA1) 1754, 1690 (OXA4)	1.2417 (PRA1)	1616 (PRA1)	1.0136 (PRA1), 1.0149 (PRA2)	3439 (PRA1), 3421 (PRA2)

Each molecule of paracetamol-oxalic acid cocrystal has three hydroxyl groups, one belongs to paracetamol and the other two are of oxalic acid. In the observed spectra of cocrystal the stretching modes of the hydroxyl groups of the paracetamol and oxalic acid are observed at 3383/3380 cm^{-1} in IR/Raman spectra and at 2999 cm^{-1} in the IR spectra respectively, which indicates that all the hydroxyl groups are hydrogen bonded. However, in the monomer of PRA-OXA cocrystal (Fig.1) the hydroxyl group of paracetamol molecule and one of the hydroxyl groups of oxalic acid are free. As such to get a better picture of the effect of hydrogen bonding on vibrational spectra the calculations were also performed on dimer+2OXA (Fig.2-having two paracetamol and four oxalic acid molecules) in which all the three hydroxyl groups, are hydrogen bonded to the neighboring molecules, giving better agreement with experimental spectra.

All the assigned wavenumbers of the intense vibrational modes of cocrystal calculated using monomer and dimer+2OXA models and assignments along with the PED are given in TableS4, ESI†. Experimental and theoretical bond length and stretching wavenumber of bonds involved in hydrogen bonding are shown in Table1. Comparison of the calculated (scaled) IR and Raman spectra of monomer and dimer+2OXA with the observed spectra is shown in Fig.3 and Fig.4. Comparison of experimental and calculated (scaled) IR and Raman spectra of paracetamol and oxalic acid are given in Fig. S5, S6, S7 and S8, ESI†.
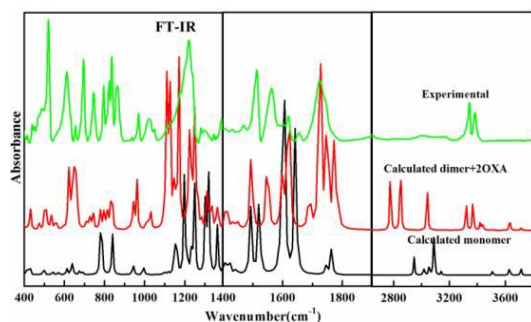
Fig.3 Experimental and calculated (scaled) IR absorbance spectra of PRA-OXA cocrystal in the region 400-1389 cm^{-1},1400-1900 cm^{-1} and 2600-3800 cm^{-1}
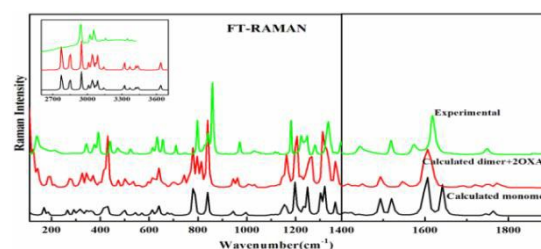
Fig. 4 Experimental and calculated (scaled) Raman scattering spectra of PRA-OXA cocrystal in the region 100-1389 cm^{-1},1400-1900 cm^{-1} and 2600-3700 cm^{-1}.

4.2.1 OH group of Paracetamol

The O-H stretching vibrations are sensitive to hydrogen bonding. The non-hydrogen bonded (or) free hydroxyl group absorbs strongly in 3700-3550 cm^{-1} region. Whereas the existence of H-bonding can lower the O-H stretching vibration to the region 3500–3200 cm^{-1} region with increase in IR intensity and breadth[44,45].

Hydroxyl group of paracetamol is forming a weaker hydrogen bond in cocrystal than the pure paracetamol (API), which is reflected in the smaller OH bond length and higher OH stretching frequency in cocrystal as shown in Table1. This hydroxyl OH stretching mode calculated in monomer at 3712 cm^{-1} shows a red shift[46], while in dimer+2OXA this mode is computed at 3320 cm^{-1} which is closer to the observed value at 3383/3380 cm^{-1} in IR /Raman spectra of cocrystal as shown in Table S4. This downward shift in the calculated wave number corresponds to an increase in bond length of OH, which is 0.963 Å in monomer and 0.984 Å in dimer+2OXA. In monomer the hydroxyl group of paracetamol is free while in dimer+2OXA it is forming intermolecular hydrogen bond with neighboring oxalic acid molecule.

4.2.2 OH group of oxalic acid

There are two hydroxyl groups in oxalic acid both having bond length 0.9257 Å as shown in Fig. S9 ESI†,. However, in case of cocrystal, these hydroxyl group have bond length 0.9827 Å and 0.9823 Å, forming strong hydrogen bonding with the C=O groups of paracetamol and oxalic acid of neighboring cocrystal molecule, respectively (as shown in Fig. 2).

The observed IR stretching frequency of O-H group is 3099 cm^{-1} and 2999 cm^{-1} in oxalic acid and cocrystal respectively, suggest that hydroxyl group stretching of oxalic acid in cocrystal is red shifted due to stronger hydrogen bonding as shown in Fig. 3. The calculated OH stretching mode in monomer at 3086 cm^{-1} shows a red shift in dimer+2OXA and occurs at 2777 cm^{-1}. This downshift in wavenumber corresponds to an increase in calculated O-H bond length, which is 0.998 Å in monomer and 1.016 Å in dimer+2OXA. The O10····H28-O25 hydrogen bond is strongest among all of the H-bond as O25-H28 bond length turns out to be longest among all the H-bond in PRA-OXA. The larger O-H bond length and corresponding lowering of the OH stretching frequency unambiguously indicate that hydrogen bonding leads to a redistribution of the electron density.

4.2.3 Amide group

The positions of N-H stretching bands are dependent on the strength of hydrogen bond formed. The free N-H stretching modes of secondary amides are generally observed in the region 3460–3300 cm^{-1}.[47]

In case of paracetamol NH is forming hydrogen bond with the OH group of neighboring molecule as shown in Fig. S10, ESI†. However, in case of cocrystal NH group is hydrogen bonded with the carbonyl group of oxalic acid and as such the hydrogen bonding pattern of API is completely different from cocrystal. The corresponding hydrogen bond is weaker in cocrystal in comparison to the paracetamol as the observed bond length of NH in larger in paracetamol as shown in Table1. The N-H stretching frequency is observed at 3256 cm^{-1} in IR spectra of paracetamol and at higher value 3344/3346 cm^{-1} in IR/Raman of cocrystal as shown in Fig. 3 whereas it is calculated at 3509 cm^{-1} in monomer and 3421 cm^{-1} in dimer+2OXA. This decrease in calculated wavenumber is attributed to increase in the bond length of N-H by 0.005 Å, due to incorporation of intermolecular N-H····O interactions[48] in dimer+2OXA, which was not taken into account in case of monomer. This also resulted in better agreement of the calculated N-H stretching mode of dimer+2OXA, with the observed spectra. The observed N-H rocking mode at 1514 /1519 cm^{-1} in IR/Raman spectra of cocrystal is in good agreement with the calculated wave number 1521 cm^{-1} in monomer as shown in Table S4. The calculated N-H wagging mode at 541 cm^{-1} is assigned to the observed IR/Raman peak at 521 cm^{-1} / 524 cm^{-1}.

The C=O stretching mode is observed at 1655 cm^{-1} in IR spectra of cocrystal. In paracetamol this mode is observed at 1651/1649 cm^{-1} in IR/Raman spectra. The stretching mode of C=O group is calculated at 1643 cm^{-1} in monomer and 1616 cm^{-1} in dimer+2OXA. This implies that C=O mode is involved in intermolecular hydrogen bonding as the bond length of C=O mode increases by 0.008 Å in dimer+2OXA as compared to monomer. The stretching vibration of CN is calculated at 1233 cm^{-1} corresponding to the observed peak at 1221/1223 cm^{-1} in the IR/Raman spectrum and the torsion mode of CN is calculated at 610 cm^{-1} and observed at 611/615 cm^{-1} in IR/Raman spectrum.

4.2.4 C=O group of oxalic acid

The most of the characteristic features of the carboxylic group are observed usually in 1750–1600 cm^{-1} regions[49]. Carboxyl group of oxalic acid is forming stronger hydrogen bond with the hydroxyl group of paracetamol in cocrystal in comparison to pure oxalic acid as the bond length of C=O of oxalic acid molecule in cocrystal is higher (1.23929 Å) than in pure oxalic acid (1.20707 Å). As such, corresponding stretching frequency is observed at 1724 cm^{-1} in IR of cocrystal and 1749 cm^{-1} in IR of oxalic acid. Whereas C=O stretching mode is calculated at 1764 cm^{-1} in monomer, shows a red shift in dimer+2OXA and calculated at 1690 cm^{-1}, which is in better agreement with the experimental spectra as shown in Table1. In dimer+2OXA the C=O group of oxalic acid is involved in intermolecular hydrogen

bonding with the hydroxyl group of paracetamol (as shown in Fig.2).

4.2.5 Ring Vibrations

The C-H stretching mode of aromatic compound appears in the range 3100-3000 cm^{-1} [50,51]. The ν(CH) stretching vibration of the ring is calculated at 3057 cm^{-1} corresponding to the observed values 3051/3055 cm^{-1} in IR/Raman spectra as shown in Table S4. The C-H in plane bending frequencies appear in the range 1350-1000 cm^{-1} [52] and very useful for characterization purpose. This mode is calculated at 1098 cm^{-1} that corresponds to the observed values at 1115/1116 cm^{-1} in IR/Raman spectra. The C-H out-of-plane bending vibrations are strongly coupled vibrations and occur in the region 900-667 cm^{-1} [53]. Out-of-plane vibration δ_{out} (CH) is calculated at 814 cm^{-1} corresponding to the observed peak at 823/828 cm^{-1} in IR/Raman spectrum having almost equal intensity. The carbon–carbon stretching modes are expected in the range from 1650 to 1200 cm^{-1}. The ring ν (CC) stretching is calculated at 1603 cm^{-1} corresponding to the observed IR/Raman peak at 1620/1618 cm^{-1}. The stretching vibration of C1N8 is calculated at 1199 cm^{-1} and observed at 1178/1182 cm^{-1} in IR/Raman spectrum. Puckering mode of the ring is calculated at 689 cm^{-1}, corresponds to the observed band at 696/709 cm^{-1} in the IR/Raman spectra. The asymmetric deformation is calculated at 637 cm^{-1} and observed at 633 cm^{-1} in Raman spectra. Asymmetric torsion is calculated at 406 cm^{-1} and assigned to the peak at 415/392 cm^{-1} in the IR/Raman spectrum.

4.2.6 Methyl group vibrations

The methyl group vibrations are localized and not much effected by the formation of cocrystal. The asymmetric stretching vibration of CH$_3$ group is calculated at 3022 cm^{-1} corresponding to the observed IR/Raman peak at 3024/3020 cm^{-1} while symmetric stretching is calculated at 2947 cm^{-1} and assigned to the observed peaks at 2945/2941cm^{-1} in IR/Raman spectrum as shown in Table S4. Its asymmetric deformation is calculated at 1444 cm^{-1} and observed at 1446/1444 cm^{-1} in the IR/Raman spectrum. The rocking mode ρ(CH$_3$) is calculated at 1021 cm^{-1} and assigned to the observed peak at 1022 cm^{-1} in IR and at 1030 cm^{-1} in Raman spectrum.

4.3 Natural bond orbital analysis (NBO)

The NBO analysis provides an accurate method for studying interactions, intramolecular and intermolecular hydrogen bonding and provides an efficient basis for evaluating charge transfer or hyperconjugative interaction in molecular systems[54]. First order density matrix of the *ab initio* calculations was extracted to develop a unique set of atomic hybrids and bond orbital's which leads to ''Lewis structure''. It helps to understand the bonding in molecules. Delocalization of electron density between occupied, Lewis-type (bond or lone pair) NBO and formally unoccupied (anti-bond or Rydberg) non-Lewis NBO's correspond to a stabilizing donor–acceptor interaction helps in the investigation of intermolecular/intramolecular interactions among bonds, which are presented in Table 2.

The hyperconjugative interactions are formed by the orbital overlap between π(C-C) bond orbital to π*(C-C) anti-bonding orbital, which results in intramolecular charge transfer causing the stabilization of the ring with the maximum energy of 22.03 kcal/mol. On the other hand, a very strong interaction has been observed between the lone pair LP(1) (N8) and π*(C9-O10) with energy of 66.59 kcal/mol, is responsible for the stabilization of the cocrystal. Hence this lone pair also participates in LP(1)(N8)→π*(C1-C2) interaction with energy of 29.56 kcal/mol. Since π orbitals have lower occupancies than σ orbital correspondingly showing more electron- donating ability in comparison to σ orbital. This also shows that [LP(1) (N8) → π*(C9-O10)] is the most intensive interaction between the acceptor and donor which results in the molecular stability. The other weak interactions are due to O22, O23, O25 and O26

oxygen atoms as shown in Table 2. The interactions between lone pair of LP(2)(O25)→π*(C24-O26) and LP(2)(O22)→π*(C21-O23) leads to stabilization of energy 50.38 and 43.09 kcal/mol, respectively are responsible to the stabilization of molecule. The interaction LP(2)(O10)→σ*(O25-H28) confirms the hydrogen bond interaction.

Hence the charge transfer interactions are formed by the orbital overlap between bonding (π) and anti-bonding (π*) orbital's, which results in intramolecular charge transfer (ICT) causing stabilization of the system. This movement of π electron cloud from donor to acceptor i.e. ICT makes the molecule more polarized.

Table 2 Second-order perturbation theory analyses of the Fock Matrix, in the NBO basis for interactions in monomer within dimer+2OXA of cocrystal

Donor NBO (i)	ED(i)/e	Acceptor NBO (j)	ED(j)/e	$E(2)^a$ (kcal/mol)	$E(j)-E(i)^b$ (a.u.)	$F(i,j)^c$ (a.u.)
paracetamol						
πC1-C2	1.65475	π* C3-C4	0.38528	18.17	0.28	0.065
πC1-C2	1.65475	π*C5-C6	0.34188	21.34	0.28	0.069
πC3-C4	1.65259	π*C1-C2	0.38785	22.03	0.29	0.072
πC3-C4	1.65259	π*C5-C6	0.34188	18.33	0.29	0.065
πC5-C6	1.72207	π*C1-C2	0.38785	17.72	0.29	0.066
πC5-C6	1.72207	π*C3-C4	0.38528	19.98	0.28	0.069
LP(1)O7	1.97928	σ *C3-C4	0.02695	6.04	1.17	0.075
LP(2)O7	1.87948	π*C3-C4	0.38528	27.22	0.35	0.094
LP(1)N8	1.64840	π*C 1-C2	0.38785	29.56	0.31	0.086
LP(1)N8	1.64840	π*C9 -O10	0.33015	66.59	0.28	0.122
LP(2)O10	1.86095	σ *N8-C9	0.06430	22.95	0.77	0.121
LP(2)O10	1.86095	σ *C9- C11	0.04588	11.98	0.67	0.082
paracetamol to						
oxalic acid						
LP(1)O10	1.95343	σ *O25-H28	0.08706	9.50	1.02	0.089
LP(2)O10	1.84964	σ *O25-H28	0.08706	32.10	0.70	0.136
oxalic acid						
LP(1)O22	1.97683	σ * C21-O23	0.02553	6.74	1.23	0.081
LP(2)O22	1.81017	π*C21-O23	0.19728	43.09	0.36	0.112
LP(2)O23	1.84071	σ * C21-O22	0.09551	32.26	0.63	0.129
LP(2)O23	1.84071	σ *C21-C24	0.12826	21.84	0.60	0.103
LP(1)O25	1.96836	σ *C24-O26	0.02806	8.90	1.19	0.092
LP(2)O25	1.77830	π* C24-O26	0.22211	50.38	0.35	0.118
LP(2)O26	1.84235	σ *C 21-C24	0.12826	23.61	0.59	0.106

^{a}E(2) means energy of hyper conjugative interaction (stabilization energy), ^{b}Energy difference between donor (i) and acceptor (j) NBO orbital, ^{c}F(i,j) is the Fock matrix element between i and j NBO orbitals

The second-order perturbation theory analyses of the Fock Matrix, in the NBO basis for intermolecular interactions in PRA-OXA (dimer+2OXA) cocrystal are presented in Table 3. In dimer+2OXA intermolecular charge transfer from LP(1)(O7)→σ*O38-H43 stabilize the molecule with the interaction energy 16.86 kcal/mol. Another weak interaction

charge transfer due to LP(1)(O31)→σ*O7-H16 confirms the presence of charge transfer interaction O7-H16···O31 which stabilize the molecule with the energy 9.38 kcal/mol. In the similar way the interaction from LP(1)(O26)→σ*N60-H69 stabilize the molecule with the energy 4.79 kcal/mol.

Table 3 Second order perturbation theory analysis of the Fock matrix in the NBO basis for the intermolecular interactions for dimer+2OXA of cocrystal

Donor NBO (i)	ED(i)/e	Acceptor NBO (j)	ED(j)/e	$E(2)^a$ (kcal/mol)	$E(j)-E(i)^b$ (a.u.)	$F(i,j)^c$ (a.u.)
LP(1)O7	1.93717	σ *O38-H43	0.06581	16.86	0.94	0.113
LP(2)O7	1.88141	σ *O38-H43	0.06581	10.56	0.72	0.079
LP(1)O26	1.97264	σ *N60-H69	0.02393	4.79	1.15	0.066
LP(1)O31	1.95766	σ *O7-H16	0.04635	9.38	1.37	0.101
LP(2)O31	1.85914	σ *O7-H16	0.04635	4.63	0.95	0.061
σ O38-H43	1.98316	σ *C63-H72	0.00635	4.76	6.34	0.156
σC61-C63	1.98396	σ *C9-C11	0.04298	8.18	1.57	0.102
σC63-H70	1.97757	σ *O7-H16	0.04635	5.92	1.15	0.074
σC63-H70	1.97757	σ *C9-C11	0.04298	11.35	1.43	0.114
σC63-H71	1.98651	σ *C9-C11	0.04298	6.74	1.44	0.088
σC63-H72	1.96994	σ *O7-H16	0.04635	13.51	1.14	0.111
σC63-H72	1.96994	σ *C9=O10	0.02243	6.69	1.15	0.078
σC63-H72	1.96994	σ *C9-C11	0.04298	25.91	1.42	0.172

Selected Lewis orbitals (occupied bond orbital) for monomer of cocrystal with percentage ED over bonded atoms (ED_X, ED_Y in %), hybrid NBOs with s and p character are listed

in Table S5, ESI†. The NBO hybrid orbital analysis shows that all the N-H/C-N and O-H/C-O bond orbitals are polarized towards the nitrogen (ED=71.93% at N) and oxygen

(ED=79.34% at O) respectively. The electron density distribution (occupancy) around the loan pair of oxygen atoms also influences the polarity of the molecule. Therefore, they consist with the maximum electron density on the oxygen atoms, which is responsible for the polarity of molecule.

4.4 AIM calculation: Topological parameters at bond critical points (BCP)

The AIM method gives the opportunity to get an insight into a region of a system. The theory of AIM efficiently describes H-bonding and its concept without border. Bond critical point is used in the recognition of chemical bonds and strength between atoms. Geometrical and topological parameters are useful as tools to characterize the strength and nature of the H-bond. The geometrical criteria for the existence of hydrogen bond are as follows: (i) The distance between proton (H) and acceptor (A) is less than the sum of their van der Waal's radii of these atoms. (ii) The 'donor (D) proton (H)····acceptor (A)' angle is greater than 90°. (iii) The elongation of 'donor (D) proton (H)' bond length is observed. As the above criteria are frequently considered as insufficient, the existence of hydrogen bond could be supported further by Koch and Popelier criteria[55] based on 'Atoms in Molecules' theory (i) the existence of bond critical point for the 'proton (H)····acceptor (A)' contact as a confirmation of the existence of hydrogen bonding interaction. (ii) The value of electron density ($\rho_{H····A}$) should be within the range 0.002–0.040 a.u. (iii) the corresponding Laplacian $^2\rho$ (r_{BCP}) should be within the range 0.024–0.139 a.u. The criteria provide a basis to distinguish these interactions from van der Waals interactions and have been proved to be valid for standard and non-conventional H-bonds.

According to Rozas et al.[56] the interactions may be classified as follows: (i) for strong H-bonds ($\nabla^2\rho_{BCP}$) < 0, H_{BCP}< 0 and covalent in nature, (ii) for medium H-bonds($\nabla^2\rho_{BCP}$) > 0, H_{BCP}< 0 and partially covalent in nature and (iii) for weak H-bonds ($\nabla^2\rho_{BCP}$) > 0 and H_{BCP}>0 and electrostatic in nature. The van der Waals interactions are characterized when the distance between interacting atoms is greater than the sum of van der Waals radii of these atoms. Molecular graph of monomer and

dimer+2OXA of cocrystal calculated using AIM program at B3LYP/6-311++G (d,p) level is shown in Fig.S11, ESI† and Fig.5.Geometrical as well as topological parameters for bonds of interacting atoms are given in Table4. The geometrical parameters for hydrogen bonds in dimer+2OXA model are given in Table S6, ESI†. On the basis of these parameters, O7····H43, O39····H35, O31····H16, O26····H69 and O50····H17, all are medium hydrogen bonds. The Bader's theory[57] is used to estimate hydrogen bond energy (E). Espinosa[58] proposed proportionality between hydrogen bond energy (E) and potential energy density (V_{BCP}) at H··O contact: E= (1/2)(V_{BCP}). The calculated interaction energy at BCP indicates that O7····H43, O10····H28, O62····H63 and O31····H16 are strong. However O50····H17 and O26····H69 are moderate in nature whereas rest is weaker interactions.
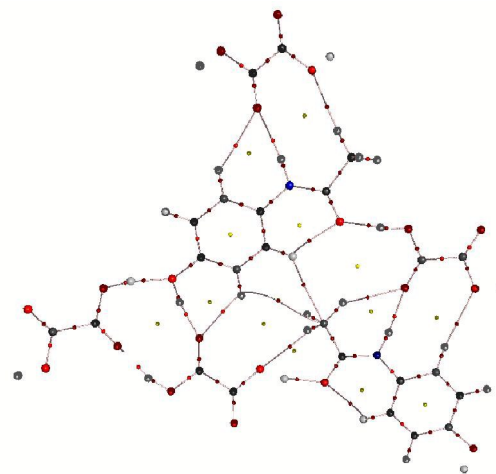
Fig.5 Molecular graph of dimer+2OXA of cocrystal: bond critical points (small red spheres), ring critical points (small yellow sphere), bond paths (pink lines).

Table 4 Geometrical parameter (bond length) and topologicalparameters for bonds of interacting atoms of PRA-OXA (dimer+2OXA): electron density (ρ_{BCP}), Laplacian of electron density ($\nabla^2\rho_{BCP}$), electron kinetic energy density (G_{BCP}), electron potential energy density (V_{BCP}), total electron energy density (H_{BCP}) at bond critical point (BCP) and estimated interaction energy (E_{int}).

Interactions	Bond length (A⁰)	ρ_{BCP} (a.u.)	$\nabla^2\rho_{BCP}$ (a.u)	G_{BCP} (a.u.)	V_{BCP} (a.u.)	H_{BCP} (a.u.)	E_{int} (kcal/mol)
O10····H28	1.51062	0.07255	0.13747	0.02711	−0.08859	−0.06148	−27.79730
O7····H43	1.52718	0.06972	0.14126	0.02631	−0.08795	−0.06163	−27.59588
O62····H36	1.56668	0.06529	0.12822	0.02472	−0.08150	−0.05678	−25.57219
O31····H16	1.61832	0.05387	0.14080	0.01785	−0.07090	−0.05305	−22.24738
O26····H69	1.84885	0.03099	0.12493	0.00439	−0.04002	−0.03563	−12.55847
O50····H17	1.95331	0.02416	0.10973	0.00106	−0.02955	−0.02849	−9.27413
O62····H64	2.17845	0.02018	0.09513	−0.00172	−0.02033	−0.02206	−6.38136
O10····H12	2.18042	0.02010	0.09538	−0.00177	−0.02030	−0.02207	−6.36912
O31····H13	2.35423	0.01159	0.06271	−0.00284	−0.00999	−0.01283	−3.13655
O26····H71	2.37670	0.01096	0.05809	−0.00274	−0.00903	−0.01177	−2.83379
O46····H19	2.40090	0.00964	0.05326	−0.00280	−0.00771	−0.01051	−2.41901
O22····H67	2.51199	0.00689	0.04108	−0.00272	−0.00481	−0.00754	−1.51196
O50····H15	2.54456	0.00683	0.03921	−0.00249	−0.00480	−0.00730	−1.50851

4.5 Chemical reactivity

Theoretically, the chemical reactivity of a molecule can be described in three ways, by using (i) MEPS map (ii) frontier orbital analysis and (iii) electronic reactivity descriptors. All calculations are performed on paracetamol (monomer) and monomer as well as dimer+2OXA forms of cocrystal, to understand the role of intermolecular interactions in affecting the chemical reactivity of individual molecule in cocrystal.

4.5.1 Molecular electrostatic potential

MEP serves as a useful quantity to investigate the molecular structure with its physiochemical property relationship[59-64]. It

correlates with the dipole moment, electro negativity, partial charges and site of chemical reactivity of the molecule.

The different values of the electrostatic potential at the surface are represented by different colors: red represents the region of negative electrostatic potential, blue represents the region of most positive electrostatic potential and green represents the region of zero potential. Potential increases in the order red < orange < yellow < green < blue. The color code of MEP map is in the range between −0.0627 a.u. to +0.0627 a.u, −0.0733 a.u to +0.0733 a.u and −0.128 a.u to +0.128 a.u. in paracetamol (monomer), PRA-OXA (monomer) and PRA-OXA (dimer+2OXA), respectively. Such mapped MEPS are shown in Fig. S12, Fig. S13, ESI† and Fig. 6, respectively. According to

the results blue shade is mainly over hydroxyl and NH group of paracetamol (monomer) and PRA-OXA (monomer), which are major neuclophilic centers, and red shade is localized over carbonyl group of paracetamol (monomer) and in case of PRA-OXA (monomer) red shade is mainly over both the carbonyl groups of oxalic acid, which are major electrophilic centre. The reduction in the electrostatic potential around oxygen atom of the amide group of paracetamol and hydrogen atom of hydroxyl group of oxalic acid is responsible for the formation of hydrogen bonding in cocrystal. Molecular docking studies of paracetamol with cyclooxygenase-2 (COX2) inhibitor also confirm (NH) of amine and (OH) of hydroxyl group[65,66] as binding sites.
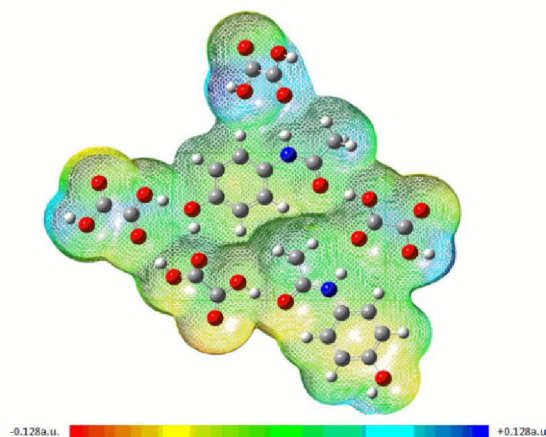
Fig. 6 Molecular electrostatic potential (MEP) formed by mapping of total density over electrostatic potential in gas phase for PRA-OXA (dimer+2OXA) of cocrystal.

In MEP map of PRA-OXA (dimer+2OXA) the region of positive electrostatic potential (blue) and electronegative potential (red) are associated with the hydroxyl and carbonyl groups of oxalic acid respectively.

4.5.2 Frontier orbital analysis

Frontier molecular orbital's (HOMO and LUMO) and their properties such as energy are used to define several types of reactions and for predicting the most reactive position in conjugated systems[67]. The energy of HOMO (E_{HOMO}) is directly related to ionization potential and energy of LUMO (E_{LUMO}) is directly related to electron affinity. According to FMO (Frontier molecular orbital theory), formation of transition state occur due to an interaction between the frontiers orbitals (HOMO and LUMO) of reactant. They are the main orbitals that take part in chemical stability[68]. The HOMO-LUMO energy gap ($\Delta E = E_{LUMO} - E_{HOMO}$) is an important stability index and also determines the

electron transport properties[69,70]. The features of HOMO-LUMO of paracetamol (monomer), cocrystal (monomer and dimer+2OXA models) can be seen in Fig. S14, Fig. S15, ESI† and Fig. 7 respectively and their energy band gaps are found to be, 5.23057 eV, 4.94893 eV and 2.4912 eV respectively.

A small gap implies low stability and large gap implies high stability. A molecule with a small HOMO-LUMO gap is more polarizable (reactive), and is generally associated with a high chemical reactivity (less stable)[71-73]. The stability of molecule can also be related to hardness, the lower stability indicates that the molecule is softer and hence more reactive. This can be confirmed from Table 5, where the value of global softness is highest for dimer+2OXA model and global hardness is highest for paracetamol. This partly explains the superior compactibility of PRA-OXA cocrystal as compared to paracetamol[12]. So, chemical reactivity of cocrystal using dimer+2OXA model is higher than the one calculated with monomer model and for paracetamol. However, the global reactivity descriptors calculated using both dimer+2OXA and monomer model indicate that cocrystal is chemically more active than paracetamol.
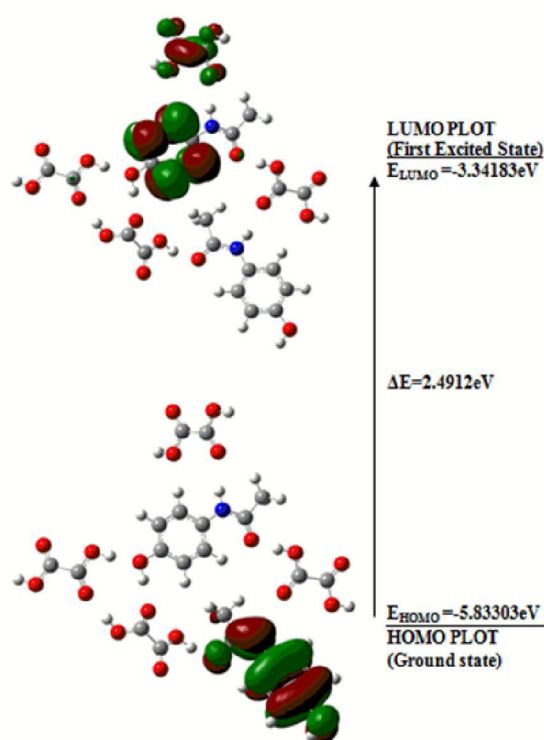
Fig.7 HOMO-LUMO plot of dimer+2OXA of cocrystal with orbital involved in electronic transitions

Table 5 Calculated E_{HOMO}, E_{LUMO}, energy band gap ($E_L - E_H$), chemical potential (μ), electro negativity (χ), global hardness (η), global softness (S) and global electrophilicity index (ω) at 298.15 K for PRA-OXA (dimer+2OXA), PRA-OXA (monomer), paracetamol (monomer) and oxalic acid (monomer).

Molecule	E_H (eV)	E_L (eV)	$E_L - E_H$ (eV)	χ (eV)	μ (eV)	η (eV)	S (e/V)	ω (eV)	ΔN_{max}
PRA-OXA (dimer+2OXA)	−5.8330	−3.3418	2.4912	4.5874	−4.5874	1.2456	0.4014	8.4475	3.6829
PRA-OXA (monomer)	−6.3119	−1.3630	4.9489	3.8375	−3.8375	2.4745	0.2021	2.9756	1.5508
paracetamol (monomer)	−5.9193	−0.6887	5.2306	3.3040	−3.3040	2.6153	0.1912	2.0870	1.2633
oxalic acid (monomer)	−7.8589	−2.1176	5.7413	4.9883	−4.9883	2.8707	0.1742	4.3339	1.7376

4.5.3. Electronic reactivity descriptors

4.5.3.1 Global reactivity descriptors

The energies of frontier molecular orbitals (E_{HOMO}, E_{LUMO}), energy band gap ($E_{LUMO} - E_{LUMO}$), electro negativity (χ), chemical potential (μ), global hardness (η), global softness (S) and global electrophilicity index (ω)[74-78] of paracetamol

(monomer), oxalic acid (monomer), PRA-OXA (monomer and dimer+2OXA) have been listed in Table 5. This new reactivity index (ω) evaluates the stabilization in energy when the system gains an additional electronic charge $\triangle N$ from the surroundings. The electronic chemical potential measures the direction of charge transfer as an electrophile is a chemical species capable of accepting electrons from the surroundings. Hence, its energy must decrease upon accepting electronic charge and its chemical potential must become negative. The calculated higher value of ω shows that the dimer+2OXA behave as a strong electrophile in comparison to monomer in cocrystal as shown in Table5. The lower energy band gap and higher value of softness of cocrystal calculated using dimer+2OXA model as well as monomer indicates that it is more reactive and softer in than paracetamol.

4.5.3.2 Electrophilicity based charge transfer (ECT) descriptors

Electrophilic charge transfer (ECT) $=(\Delta N_{max})_A - (\Delta N_{max})_B$ is defined as the difference between ΔN_{max} values of interacting molecules A and B. From Table 5 it is found that the calculated value of ECT< 0 ($-0.4743eV$), for molecules paracetamol (A) and oxalic acid (B) indicates that charge flows from paracetamol to oxalic acid. Therefore, paracetamol act as electron donor and oxalic acid as electron acceptor. In the same way, the high value of chemical potential and low value of electrophilicity index for paracetamol also favors its neuclophilic behavior, whereas the low value of chemical potential and high value of electrophilicity index for oxalic acid favors its electrophilic behavior.

4.5.3.3. Local reactivity descriptors

Fukui indices are a measurement of the chemical reactivity, as well as an indicator of the reactive regions and the neuclophilic and electrophilic behavior of the molecule. Thus, for an atom k in a molecule, three kinds of condensed Fukui function (for nucleophilic, electrophilic and radical attack) at atom k can be obtained depending upon the type of electron transfer. Fukui function is reactive descriptor to identify neuclophilic and electrophilic attack sites in particular molecule, perhaps it is also used to recognize the electron acceptor centre and donor centre.

The calculated values of local electronic descriptors for paracetamol (monomer), cocrystal (monomer) and cocrystal (dimer+2OXA) have been listed in Table S7, S8, ESI† and Table 6 respectively. From the Table S7 and S8 ESI†, it is clear that the maximum values of all three descriptors (f_k^+, s_K^+, ωk^+) at O1 or O7 indicates that the atomic centre is more prone to neuclophilic attack in paracetamol (monomer) and cocrystal (monomer). The maximum values of all three descriptors (f_k^-, s_K^-, ωk^-) at H12 in paracetamol (monomer) and H17 in cocrystal (monomer) indicates that atomic centre is more prone to electrophilic attack. In case of dimer+2OXA as shown in Table 6. it is clear that maximum values of all the three descriptors (f_k^+, s_K^+, ωk^+) at O59 indicates that this site is more prone to neuclophilic attack and the maximum values of descriptors (f_k^-, s_K^-, ωk^-) at C48 indicates that this atomic centre is more prone to electrophilic attack.

Table 6 Reactivity descriptors as Fukui functions (fk^+, fk^-), local softnesses (sk^+,sk^-), local electrophilicity indices (ωk^+, ωk^-) for dimer+2OXA using Hirshfeld atomic charges.

Sites	f_k^+	s_k^+	ωk^+	Sites	f_k^-	s_k^-	ωk^-
1 C	0.035444	0.014227	0.299413	1 C	−0.00138	−0.00055	−0.01163
2 C	0.017296	0.006943	0.146108	2 C	0.005843	0.002345	0.049359
3 C	0.021455	0.008612	0.181241	3 C	0.009078	0.003644	0.076686
4 C	0.035606	0.014292	0.300782	4 C	0.005156	0.00207	0.043555
5 C	0.029579	0.011873	0.249869	5 C	0.001278	0.000513	0.010796
6 C	0.026809	0.010761	0.226469	6 C	−0.00544	−0.00218	−0.04598
7 O	0.035814	0.014376	0.302539	7 O	0.002475	0.000993	0.020908
8 N	0.021228	0.008521	0.179324	8 N	−0.00183	−0.00073	−0.01543
9 C	0.015422	0.00619	0.130277	9 C	0.002019	0.00081	0.017056
10 O	0.01484	0.005957	0.125361	10 O	0.006449	0.002589	0.054478
11 C	0.007574	0.00304	0.063981	11 C	0.002641	0.00106	0.02231
12 H	0.006993	0.002807	0.059073	12 H	0.003596	0.001443	0.030377
13 H	0.009322	0.003742	0.078748	13 H	0.006192	0.002485	0.052307
14 H	0.017988	0.00722	0.151954	14 H	0.000665	0.000267	0.005618
15 H	0.015354	0.006163	0.129703	15 H	−0.00815	−0.00327	−0.06886
16 H	0.008774	0.003522	0.074118	16 H	0.00227	0.000911	0.019176
17 H	0.010315	0.00414	0.087136	17 H	−0.00329	−0.00132	−0.02777
18 H	0.008792	0.003529	0.07427	18 H	0.004667	0.001873	0.039424
19 H	0.007831	0.003143	0.066152	19 H	−0.00291	−0.00117	−0.02455
20 H	0.008505	0.003414	0.071846	20 H	0.005583	0.002241	0.047162
21 C	0.001829	0.000734	0.01545	21 C	0.038835	0.015588	0.328059
22 O	−0.00589	−0.00237	−0.04978	22 O	0.022744	0.009129	0.19213
23 O	0.017369	0.006972	0.146725	23 O	0.043842	0.017598	0.370355
24 C	0.004513	0.001812	0.038124	24 C	0.033423	0.013416	0.282341
25 O	0.00901	0.003617	0.076112	25 O	0.017578	0.007056	0.14849
26 O	−0.01285	−0.00516	−0.10858	26 O	0.035449	0.014229	0.299455
27 H	0.0049	0.001967	0.041393	27 H	0.016069	0.00645	0.135743
28 H	0.001675	0.000672	0.01415	28 H	0.005724	0.002298	0.048353
29 C	0.003488	0.0014	0.029465	29 C	0.002742	0.001101	0.023163
30 O	0.010053	0.004035	0.084923	30 O	0.004481	0.001799	0.037853
31 O	−0.0039	−0.00157	−0.03295	31 O	−0.00192	−0.00077	−0.01625
32 C	0.002913	0.001169	0.024608	32 C	0.001219	0.000489	0.010298
33 O	−0.00309	−0.00124	−0.02609	33 O	−0.002	−0.0008	−0.01689
34 O	0.012186	0.004891	0.102941	34 O	0.010643	0.004272	0.089907
35 H	0.003458	0.001388	0.029211	35 H	0.001302	0.000523	0.010999
36 H	0.001187	0.000476	0.010027	36 H	0.001262	0.000507	0.010661
37 C	0.002871	0.001152	0.024253	37 C	0.036749	0.014751	0.310437
38 O	0.000656	0.000263	0.005542	38 O	0.019475	0.007817	0.164515
39 O	0.000328	0.000132	0.002771	39 O	0.037786	0.015167	0.319197
40 C	0.001427	0.000573	0.012055	40 C	0.038263	0.015359	0.323227
41 O	0.003716	0.001492	0.031391	41 O	0.024726	0.009925	0.208873
42 O	0.006639	0.002665	0.056083	42 O	0.042501	0.01706	0.359027

43	H	−0.00079	−0.00032	−0.00667	43	H	0.006544	0.002627	0.05528
44	H	0.00544	0.002184	0.045954	44	H	0.016961	0.006808	0.143278
45	C	0.000626	0.000251	0.005288	45	C	0.077426	0.031079	0.654056
46	O	−0.00763	−0.00306	−0.06443	46	O	0.041346	0.016596	0.34927
47	O	0.013287	0.005333	0.112242	47	O	0.09433	0.037864	0.796853
48	C	0.002611	0.001048	0.022056	48	C	0.085202	0.0342	0.719744
49	O	0.009159	0.003676	0.077371	49	O	0.051361	0.020616	0.433872
50	O	−0.01172	−0.00471	−0.09902	50	O	0.082987	0.033311	0.701033
51	H	0.001503	0.000603	0.012697	51	H	0.028833	0.011574	0.243567
52	H	0.003485	0.001399	0.02944	52	H	0.031703	0.012726	0.267811
53	C	0.050032	0.020083	0.422645	53	C	−0.00302	−0.00121	−0.02547
54	C	0.035082	0.014082	0.296355	54	C	0.002206	0.000885	0.018635
55	C	0.039827	0.015987	0.336439	55	C	0.005391	0.002164	0.04554
56	C	0.053166	0.021341	0.44912	56	C	0.005546	0.002226	0.04685
57	C	0.040228	0.016148	0.339826	57	C	0.002285	0.000917	0.019303
58	C	0.034708	0.013932	0.293196	58	C	−0.00362	−0.00145	−0.03057
59	O	0.065381	0.026244	0.552306	59	O	0.005958	0.002392	0.05033
60	N	0.033211	0.013331	0.28055	60	N	−0.00096	−0.00038	−0.00808
61	C	0.021078	0.008461	0.178056	61	C	−0.00124	−0.0005	−0.01044
62	O	0.035626	0.0143	0.300951	62	O	0.004211	0.00169	0.035572
63	C	0.008362	0.003357	0.070638	63	C	−0.00071	−0.00028	−0.006
64	H	0.017854	0.007167	0.150822	64	H	0.001356	0.000544	0.011455
65	H	0.023866	0.00958	0.201608	65	H	0.004417	0.001773	0.037313
66	H	0.024434	0.009808	0.206406	66	H	0.002051	0.000823	0.017326
67	H	0.018496	0.007424	0.156245	67	H	−0.00473	−0.0019	−0.03998
68	H	0.026215	0.010523	0.221451	68	H	0.004027	0.001616	0.034018
69	H	0.012657	0.005081	0.10692	69	H	−0.00206	−0.00083	−0.01742
70	H	0.00694	0.002786	0.058626	70	H	−0.002	−0.0008	−0.01686
71	H	0.005296	0.002126	0.044738	71	H	−0.00385	−0.00154	−0.0325
72	H	0.01414	0.005676	0.119448	72	H	0.002192	0.00088	0.018517

4.6. Conclusions

The structural and spectral characteristics of the paracetamol–oxalic acid cocrystal have been systematically studied by experimental and quantum chemical calculation using monomer and dimer+2OXA models. Calculations on dimer+2OXA have been performed for taking into account all the nearest neighbor H-bonding interactions that resulted in improved agreement between the calculated and observed FT-IR and FT-Raman spectra in comparison to the spectra calculated using monomer model. Structural and spectral calculations indicate that OH and NH groups form stronger hydrogen bond in paracetamol(API) with the NH and OH groups of neighboring molecule respectively comparison to cocrystal. In case of cocrystal both these groups of paracetamol are hydrogen bonded to the neighboring oxalic acid molecule, resulting in an increment in the bond length and lowering in wavenumber. Hydroxyl and carbonyl stretching modes of oxalic acid are red shifted in cocrystal in comparison to pure oxalic acid as these groups make stronger hydrogen bonding with C=O, O-H and N-H groups of paracetamol resulting in the formation of cocrystal. According to natural bond orbital (NBO) analysis, in cocrystal two types of interactions are responsible for stability of the molecule. First one is intramolecular interaction with in the paracetamol LP(1) (N8)→π*(C9-O10) and oxalic acid molecule LP(2) (O25)→π*(C24-O26) with interaction energy 66.59 kcal/mol and 50.38 kcal/mol, respectively, while the second type of interaction is due to hydrogen bond between the lone pair of paracetamol and oxalic acid LP(2)(O10)→σ*(O25-H28) and vice versa.Atom in molecule (AIM) calculation suggest that hydrogen bonds C=O····H−O in cocrystal are moderate in nature as $\nabla^2\rho_{BCP} > 0$, $H_{BCP} < 0$ with the maximum interaction energy E= −27.59 kcal/mol. From the molecular electrostatic potential (MEPS) map, it is shown that the negative and positive region is localized over carbonyl and hydroxyl groups of oxalic acid in cocrystal.Comparison of chemical reactivity parameters of paracetamol with paracetamol-oxalic acid cocrystal indicates that cocrystal is more reactive than paracetamol(API).The calculated value of electrophilic charge transfer ECT< 0 (−0.4743 eV) in cocrystal indicating that the charge flows from paracetamol to oxalic acid.

References

1. N. Schultheiss, A. Newman, *Cryst Growth Des.*, 2009, **9**, 2950–2967.
2. Ö. Almarsson, MJ. Zaworotko, *ChemCommun.*, 2004, 1889-1896.
3. J. Soleimannejad, E. Nazarnia, H. Stoeckli-Evans, *Journal of Molecular Structure.*, 2014.
4. G.R.Desiraju, J. J.Vittal, Arunachalam, Ramanan, IISC,Press.
5. G. R. Desiraju, *J. Chem. Sci.*, 2010, 667–675.
6. S Ning, J.Z. Michael, *Drug Discov Today.*, 2008,**13**,440-6.
7. RH Nair, J N Sarah, J Adivaraha, Swarbreek editors, *Informa Healthcare.*, 2007.
8. Aghababian, V. Richard , *Essentials of Emergency Medicine.*, 2010.
9. J. Ahmad, *Springer.*, 2010, p. 194.
10. a) P. Di Martino, A.-M. Guyot-Hermann, P. Conflant, M. Drache, J.-C.Guyot, *Int. J. Pharm.*, 1996, **1**, 128. b) G. Nichols, C. S. Frampton, *J. Pharm.Sci.*, 1998, **87**, 684. c) K. Kachrimanis, K. Fucke, M. Noisternig, B. Siebenhaar,U. J. Griesser, *Pharm. Res.*, 2008, **25**, 1440. d) T. Beyer, G. M. Day, S. L.Price, *J. Am. Chem Soc.*, 2001, **123**, 5086.
11. J. M. Fachaux, A. M. Guyot-Hermann, J. C. Guyot, P. Conflant, M. Drache, S.Veesler, R. Boistelle, *Powder Technol.*,1995, **82**, 123.
12. S. Karki, T. Friscic, L. Fabian, P. R. Laity, G. M. Day, W. Jones, *Adv Mater.*, 2009, **21**, 3905-3909.
13. Y. Lin, H. Yang, C. Yang, J. Wang, *Pharm Res.*, 2013.
14. S. P. Delaney and T. M. Korter, *J. Phys. Chem. A.*, 2015, **119**, 3269−3276.
15. T. Polat F. Bulut I. Arıcan F. Kandemirli G. Yildirim , *Journal of Molecular Structure.*, 2015.
16. M. M. Nolasco, A. M. Amado and P. J. A. Ribeiro-Claro,*Chem. PhysChem.*, 2006, **7**, 2150–2161.
17. P.J.A.Ribeiro-Claro, P.D.Vaz and M. Nolasco, *THEOCHEM.*, 2010, **946**, 65–69.
18. M. Sardo, A. M. Amado and P. J. A. Ribeiro-Claro, *J. Raman Spectrosc.*, 2009, **40**, 1956–1965.
19. M.J. Frisch, G.W. Trucks, H.B. Schlegel, G.E. Scuseria, J.R. Cheeseman,M.A. Robb,G. Scalmani, V. Barone, B. Mennucci,

G.A. Petersson, H. Nakatsuji, M. Caricato,X. Li, H.P. Hratchian, A.F. Izmzylov, J. Bloino, G. Zheng, J.L. Sonnenberg, M. Hada,M. Ehara, K. Toyota, R. Fukuda,J. Ishida, M. Hasegawa, T. Nakajima, Y. Honda,O. Kitao, H. Nakai, T. Vreven, J.A. Montgomery Jr., J.E. Peralta, F. Ogliaro, M.Bearpark, J.J. Heyd, E. Brothers, K.N. Kudin, V.N. Staroverov, R. Kobayashi, J. Normand, A. Raghavachari, A. Rendell, J.C. Burant, S.S. Iyengar,J. Tomasi, M.Cossi, N. Rega, J.M. Millan, M. Klene, J.E. Knox, J.B. Cross, V. Bakken, C. Adamo,J. Jaramillo, R. Gomperts, R.E. Stratmann,O. Yazyev, A.J. Austin, R. Cammi, C.Pomelli, J.W. Ochterski, R.L. Martin, K. Morokuma, V.G. Zakrzewski, G.A. Voth,P. Salvador, J.J. Dannerberg,S. Dapprich, A.D. Daniels, J. Farkas, B. Foresman, J.V.Ortiz, J. Cioslowski,D.J. Fox, GAUSSIAN 09, Revision, Gaussian, Inc., Wallingford,CT, 2009

20. G.A. Petersson, A. Bennett, T.G. Tensfeldt, M.A. Allaham, W.A. Shirley, J.Mantzaris, *J. Chem. Phys.*, 1988, **89**, 2193–2218

21. G.A. Petersson, M.A. Allaham, *J. Chem. Phys.*, 1991, **94,** 6081–6090.

22. C.T. Lee, W.T. Yang, R.G. Parr, *Phys. Rev. B.*, 1998, **37,** 785–789.

23. A.D. Becke, *J. Chem. Phys.*,1993, **98**, 5648–5652.

24. R.G. Parr, W. Yang, Density Functional Theory of Atoms and Molecules, Oxford,New York, 1989.

25. P.L. Polavarapu, *J. Phys. Chem.*, 1990, **94** ,8106–8112.

26. G.A. Guirgis, P. Klaboe, S. Shen, D.L. Powell, A. Gruodis, V. Aleksa, C.J. Nielsen, J. Tao, C. Zheng, J.R. Durig, *J. Raman Spectrosc.*, 2003, **34**, 322–336.

27. P. Pulay, G. Fogarasi, F. Pang, J.E. Boggs, *J. Am. Chem. Soc.*, 1979, **101**, 2550–2560.

28. G. Fogarasi, X. Zhou, P.W. Taylor, P. Pulay, *J. Am. Chem. Soc.*, 1992, **114**, 8191.

29. J.M.L. Martin, C.V. Alsenoy, GAR2PED, University of Antwerp, 1995

30. G.A. Zhurko, D.A. Zhurko, Chemcraft, 2005.Available from: < http:// www.chemcraftprog.com>.

31. A. Frisch, A.B. Nielson, A.J. Holder, GAUSSVIEW User Manual, Gaussian Inc.,Pittsburgh, PA, 2000.

32. R.F.W. Bader, J.R. Cheeseman, AIMPAC, 2000

33. F. Weinhold, C.R. Landis, Valency and Bonding: A Natural Bond Orbital Donor Acceptor Perspective , Cambridge University Press, New York , 2005

34. F. Weinhold, C.R. Landis, *Chem. Educ. Res Pract. Eur.*, 2001 **2**,91–104.

35. A.E. Reed, L.A. Curtiss, F. Weinhold, *Chem. Rev.*, 1988, **88**, 899–926.

36. R.G. Parr, R.G. Pearson, *J. Am. Chem. Soc.*, 1983,**105** , 7512–7516.

37. R.G. Parr and W. Yang, *J Am Chem Soc.*, 1984 ,**106**, 4049-4050.

38. R.G. Pearson, *J. Org. Chem.*, 1989, **54,** 1430–1432.

39. Y.V.Nelyubina, I.V.Glukhov, M.Yu.Antipin, K.Lyssenko, *Chem. Commun.*, 2010, **46**, 3469.

40. J.L.Derissen,P.H.Smit,*ActaCrystallogr.,Sect.B:Struct.Crystallogr. Cryst.Chem.*, 1974, **30**, 2240.

41. F. Bernardi, S.F. Boys, *Mol. Phys.*, 1973, **25**, 35.

42. Y. Danten,* T. Tassaing, and M. Besnard, *J. Phys. Chem. A.*, 2006, **110**, 8986-9001.

43. M. P. Andersson and P. Uvdal**J. Phys. Chem. A.*, 2005, **109**, 2937-2941.

44. K. Bahgat, A.G. Ragheb, *Cent. Eur. J. Chem.*, 2007, **5**, 201–220.

45. N.B. Colthup, I.H. Daily, S.E. Wiberley, Academic Press, New York, 1990

46. J. Joseph and E. D. Jemmis, *J. AM. CHEM. SOC.*, 2007, **129**, 4620-4632.

47. F.R. Dollish, W.G. Fateley, F.F. Bentley, John Wiley & Sons, New York, 1997.

48. D. Sajan, H.J. Ravindra, N. Mishra, I.H. Joe, *Vib. Spectrosc.*, 2010 , **54**, 72–80.

49. C.N. Banwell, E.M. McCash, McGraw-Hill International (UK) Limited, 1994.

50. G. Varsanyi, vols. 1 and 2, Academic Kiado, Budapest, 1973

51. M. Arivazhagan, R. Kavitha, *J. Mol. Struct.*, 2012, **1011**, 111–120.

52. N. Sundaraganesan, S. Ilakiamani, B.D. Joshua, *Spectrochim. Acta A.*, 2007 ,**67**, 287–297.

53. V. Krishnakumar, R. J. Xavier, *Indian J. Pure Appl. Phys.*, 2003, **41**, 597–601.

54. Y. Sheena Mary, C. YohannanPanicker, T. Thiemann, M. Al-Azani, A. A.Al-Saadi, C.VanAlsenoy, K. Raju, J.A. War, S K. Srivastava, *Spectrochimica Acta PartA: Molecular and Bimolecular Spectroscopy.*, 2015 .

55. U. Koch, P. Popelier, *J. Phys. Chem. A* ., 1995, **99**, 9747–9754.

56. I. Rozas, I. Alkorta, J. Elguero, *J. Am. Chem. Soc.*, 2000, **122**, 11154–11161.

57. R. F. W. Bader, 'Atoms in Molecules A Quantum Theory',Oxford University Press, Oxford, 1990

58. E. Espinosa, E. Molins, C. Lecomte, *Chem. Phys. Lett.*, 1998, **285**,170–173.

59. S. Chidangil, M.K. Shukla, P.C. Mishra, *J. Mol. Model.*, 1998, **4**,250–258.

60. I. Alkorta, J.J. Perez, *Int. J. Quantum Chem.*, 1996, **57**, 123–135.

61. E. Scrocco, J. Tomasi, in: P. Lowdin (Ed.), Advances in Quantum Chemistry, vol.2, Academic Press, New York, 1978.

62. F.J. Luque, M. Orozco, P.K. Bhadane, S.R. Gadre, *J. Phys. Chem.*, 1993, **97**,9380–9384.

63. J. Sponer, P. Hobza, *Int. J. Quantum Chem.*, 1996, **57**, 959–970.

64. J.S. Murray, K. Sen, Elsevier, Amsterdam, 1996.

65. L. FERENCZ, D.L. MUNTEAN, *FARMACIA.*, 2015.

66. M. A. Qureshi, T.J. Khan, M.S. Qureshi,*Rawal Medical Journal.*, July-September 2011.

67. L. Padmaja, M. Amalanathan, C. Ravikumar, I. Hubert Joe, *Spectrochim. Acat A.*, 2009, **74**, 349–356.

68. S. Gunasekaran, R.A. Balaji, S. Kumaresan, G. Anand, S. Srinivasan, Can. J. Anal. *Sci. Spectrosc.*, 2008, **53**,149–161.

69. P.W. Atkins, *Physical Chemistry.*, Oxford University Press, Oxford, 2001

70. K. Fukui, *Science.*, 1982, **218,** 747.

71. K. Fukui, T. Yonezawa and H. Shingu, *J. Chem. Phys.*, 1952, **20**, 722.

72. D. F. V. Lewis, C. Ioannides, D. V. Parke, *Xenobiotica.*, 1994, **24**, 401-408.

73. D. C. Ghosh, J. Jana, *Current Science.*, 1999, **4**, 76.

74. R.G. Pearson, *J. Org. Chem.*, 1989, **54**, 1430–1432.

75. P. Geerlings, F.D. Proft, W. Langenaeker, *Chem. Rev.*, 2003,**103**, 1793–1873.

76. R.G. Parr, L.V. Szentpaly, S. Liu, *J. Am. Chem. Soc.*,1999 **121**,1922–1924.

77. P.K. Chattaraj, S. Giri, *J. Phys. Chem. A* 2007, **111** , 11116–11121.

78. J. Padmanabhan, R. Parthasarathi, V. Subramaniaan, P.K. Chattaraj, *J. Phys. Chem. A* (2007), **111**, 1358–13.

Table of contents
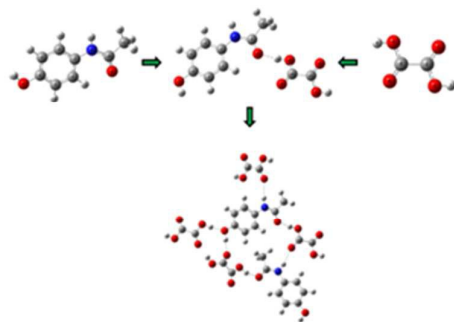
Hydrogen bonding network present in monomer and dimer+2OXA models of cocrystal.